Chapter V

3D MODELLING

5.1. Introduction

Many analogue and numerical models have been constructed in order to investigate the salt behaviour under different tectonic settings and load conditions. The modelling approaches of salt movements focussed on different aspects of salt tectonics. This includes a combination of two major effects on salt flow by: (1) fault tectonics at the base of the salt and/or overburden as a triggering mechanism; and (2) changing load distributions in time and space. The results of analogue experiments and numerical simulations demonstrate that the viscous salt is very responsive to variable sediment loading and fault tectonics (e.g. Woidt, 1978; Schmeling, 1987; Roemer and Neugebauer, 1991; Vendeville and Jackson, 1992; Koyi et al., 1993; Poliakov et al., 1993; Daudre, B., Cloetingh, S., 1994; Koyi, 1998; Kaus and Podladchikov, 2001). Most of these experiments were performed in terms of two-dimensional studies. However, three-dimensional modelling has to be used to investigate salt flow phenomena. Recently, only a few physical models have been implemented in full 3D (e.g. Guglielmo et al., 1999; Scheck et al. 2003; Ismail-Zadeh et al.; 2004). The advancement from the 2D to 3D modelling was illustrated by Guglielmo et al. (1999) who visualized the results of 2D analogue modelling into a 3D digital model, demonstrating changes of sedimentation, deformation, and underlying salt thickness through time. A full 3D numerical approach was applied by Scheck et al. (2003) for the NE German Basin, considering salt flow as a consequence of spatially changing overburden, isostatic response and sediment compaction. Ismail-Zadeh et al. (2004) investigated the evolution of salt structures both forward and backwards in time by means of 3D numerical finite-element models.

This chapter presents the results of three-dimensional modelling within the GG by using a software developed at the GeoForschungsZentrum Potsdam by Ulf Bayer, Magdalena Scheck-Wenderoth and Björn Lewerenz. The 3D reverse modelling approach has been used to determine salt distribution for selected stratigraphic levels in response to unloading due to sequential removing of the stratigraphic layers. In addition, 3D forward modelling has been applied to calculate the initial Permian salt thickness within the area covered by the 3D model. Salt flow has been determined by using a finite-element method,

depending mainly on the sedimentary load and the shape of the isostatically-balanced crust. Finite-element methods are ideal for problems with a complex geometry, which predominates among the salt structures. A basic assumption in this approach is that the behaviour of salt is similar to a viscous fluid that is usually in hydrostatic equilibrium with the overburden and that its volume is conserved. It is also assumed that all new load conditions generated by salt redistribution are isostatically compensated at the crustal level.

5.2. Analytical and numerical approaches

The 3D numerical modelling work presented here is based on some numerical approaches, which have been described in details by Scheck (1997), Scheck and Bayer (1999) and Scheck et al. (2003). Here, the conceptual definition of the salt redistribution is only elucidated.

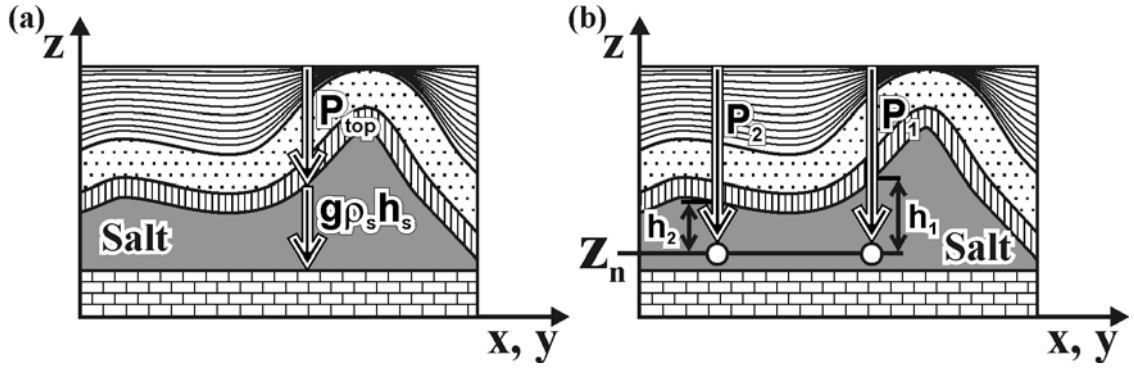

Figure 5.1. Schematic illustration of the pressure distribution in the viscous salt layer under isostatic balance (slightly modified after Scheck et al., 2003). (a) The pressure at the salt base is the sum of the load acting on the salt surface (P_{top}) and the load of the salt column ($g\rho_s h_s$). (b) The pressure difference between two points in the salt layer equals zero at the same depth (Z_n).

The model contains algorithms to simulate the changes of the salt thickness due to loading or unloading. Changes of salt thickness are calculated in response to these processes. Figs. 5.1 and 5.2 illustrate some of the parameters included in the model calculations. A typical starting condition for the modelling is shown in Fig. 5.1, demonstrating a schematic load pressure distribution in the viscous salt layer under isostatic balance. The modelled salt

layer is isostatically conditioned with an equilibrated pressure at the base of the salt *P*. *P* is the sum of the overburden load (P_{top}) and the load of the salt column $(g\rho_s h_s)$ (Fig. 5.1a).

$$P = P_{top} + g\rho_s h_s, \qquad (1)$$

where g is the gravitational acceleration, ρ_s is the salt density and h_S is the salt thickness at a predefined time.

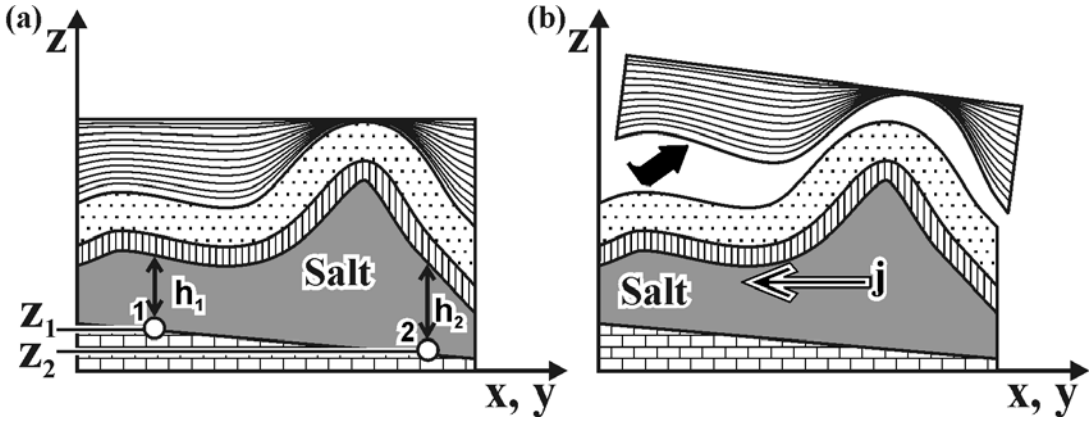

Figure 5.2. (a) Pressure balancing above the variable base topography of the salt layer. Calculation is performed by taking into account the pressure balancing for the interval between two points Z_1 and Z_2 as a reference depth. (b) Salt redistribution under new load conditions due to removing layer from top. Salt flow is characterized by the formal flux j which operates as a flow of salt towards areas of load deficit (modified after Scheck et al., 2003).

The pressure difference ΔP between two points 1 and 2 at the same depth z_n (Fig. 5.1b) can be derived according to follow equation:

$$\Delta P_{[1,2]} = P_1 - P_2 + g\rho_s(h_1 - h_2) \qquad (2)$$

This pressure difference ΔP equals zero under hydrostatic equilibrium. In case of variable base topography of the salt layer (Fig. 5.2a), Eq. (2) becomes:

$$\Delta P_{[1,2]} = 0 = P_1 - P_2 + g\rho_s(h_1 - h_2) - g\rho_s(z_1 - z_2), \qquad (3)$$

where $g\rho_s(z_1 - z_2)$ is the pressure difference between two points z_1 and z_2 due to their absolute difference in depth, representing the reference depth $(z_1 - z_2)$, which has to be taken into account during isostatic balance calculation.

When overburden is unloaded or loaded, the system becomes hydrostatically unbalanced and $\Delta P_{[1,2]} = 0$ is not satisfied. The formal flux of salt (j) is introduced (Fig. 5.2b) in order to reestablish the hydrostatical equilibrium of the system by salt redistribution in response to the new load conditions:

$$j = \Delta(P_{top}(t) + g\rho_s h_s(t) - g\rho_s Z_{base}), \qquad (4)$$

where $Z_{base} = z_i - z_{i+1}$. The system becomes again hydrostatically balanced when the flux of salt equals zero ($j=0$).

5.3. Results of 3D reverse modelling

5.3.1. Modelling concept

Salt flow can cause local or regional thickening and thinning of sediments, which represent the most prominent manifestation of salt movements in salt-containing sedimentary basins. In other words, the tectonically induced thinning (depletion) of the salt layer generates an additional accommodation space for sedimentation. On the other hand, thickening of the salt layer (formation of salt structures) generates increased surface topography, causing a shortage of sedimentation space. In contrast, the 3D reverse modelling represents an inverse process when thinning and thickening of the salt layer occur due to unloading of the model by removing of layers (Fig. 5.3).

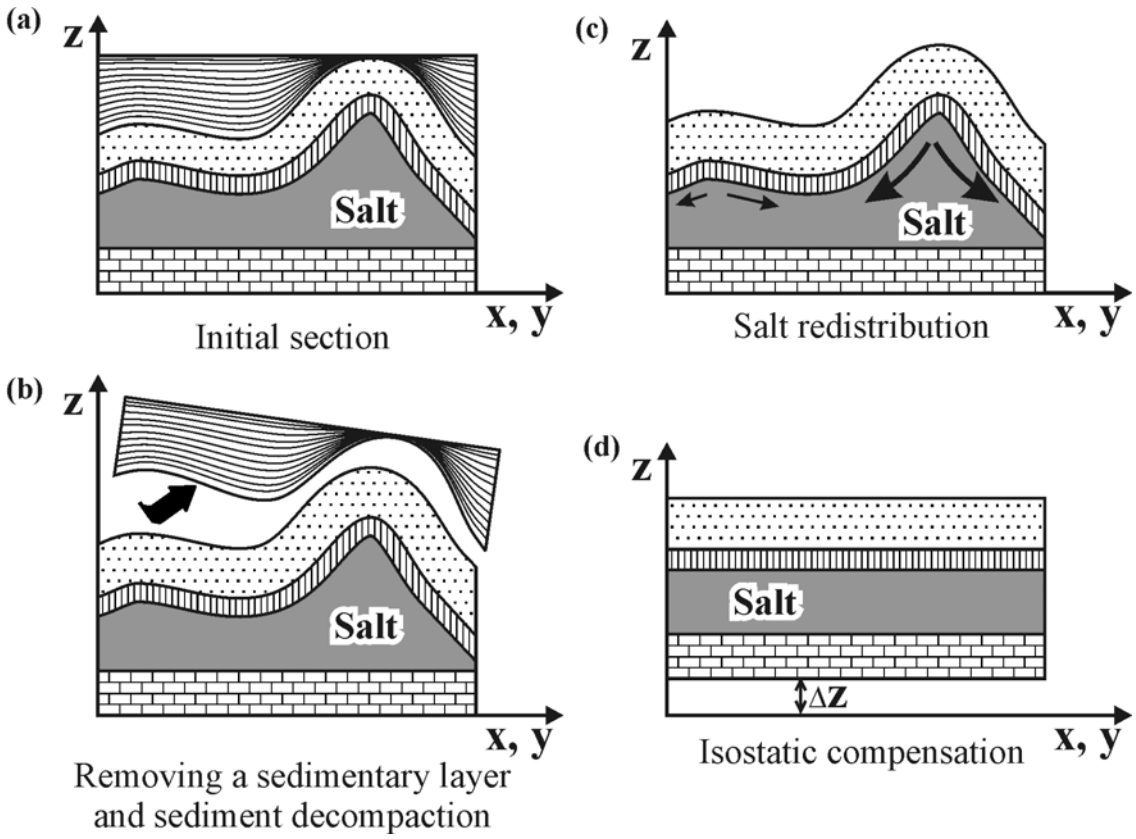

Figure 5.3. Schematic diagram showing steps of the reverse modelling from the initial state to the selected stratigraphic level (modified after Scheck et al., 2003).

A 3D reverse modelling of the development of salt structures consists of a number of steps which are illustrated by the schematic two-dimensional diagram in Fig. 5.3. The section in Fig. 5.3a corresponds to the present state of the model. The first step is to remove the sediments above the selected stratigraphic level (Fig. 5.3b). Sediment decompaction is the next culculated. An exponential decrease in porosity under loading for each lithology is used for decompaction according to decompaction parameters which are given in Table 5.1. Subsequently, the new distribution of the salt is calculated under reduced sediment load of the remained layers above the salt (Fig. 5.3c). Finally, an isostatic equilibrium of the model is recalculated according to the new mass distribution. The new mass distribution includes both the unloading of the model due to removing of sediments, and loading/unloading by the new thickness of salt (Fig. 5.3d). The described sequence of the modelling procedures was applied to every step of backstripping, which has been used to reconstruct a reasonable geometry of salt structures from present day to the end of the Triassic.

Stratigraphic layer	Matrix density ρ_m (kg/m^3)	Initial porosity Φ_o (%)	Compaction depth constant c (1/km)
Quaternary-Neogene	2690	58	0,43
Paleogene	2710	65	0,57
Upper Cretaceous	2700	67	0,68
Lower Cretaceous	2715	65	0,59
Jurassic	2690	58	0,33
Triassic	2684	53	0,47
Permian salt	2300	0	0,00
Pre-Permian crust	2850	0	0,00
Mantle	3300	0	0,00

Porosity Φ is assumed to decrease under loading according to $\Phi = \Phi_{min} + (\Phi_o - \Phi_{min})e^{-\beta P}$, where Φ_{min} is the minimum porosity at the maximum depth (assumed to be 0 for all layers), Φ_o is the porosity on the surface (initial porosity), P is the effective load, and β is given as $\beta = c/g\rho_r$, where c is compaction depth constant, g is the gravitational acceleration and ρ_r is the matrix density.

Tabl. 5.1. Decompaction parameters of rocks for the different layers of the 3D model within the GG. These parameters were calculated according to lithological composition of rocks, which is shown in Fig. 1.5.

5.3.2. Reconstruction of the initial distribution of sediments

Modelling difficulties arise when input data contain layers, which were affected by postdepositional changes. Such changes occur as a result of several geological processes. One process is erosion due to salt tectonics, regional uplift or sea level fall. Simple removing of the upper layers above partially eroded stratigraphic interval does not produce proper load conditions, which existed before erosion. Therefore, salt redistribution will not provide a correct geometry for this stratigraphic interval. Scheck et al. (2003) solved this problem by

reestablishment of initial sediments distribution. The concept for a particular case is illustrated in Fig. 5.4 where two sedimentary layers are pierced by a salt diapir after deposition. At first, all pierced layers have to be removed before salt redistribution (Fig. 5.4b). The next step is the reestablishment of the restored distribution of sediments into the model in order to obtain a correct load distribution above the salt diapir (Fig. 5.4c). Only after that step, salt can be correctly redistributed.

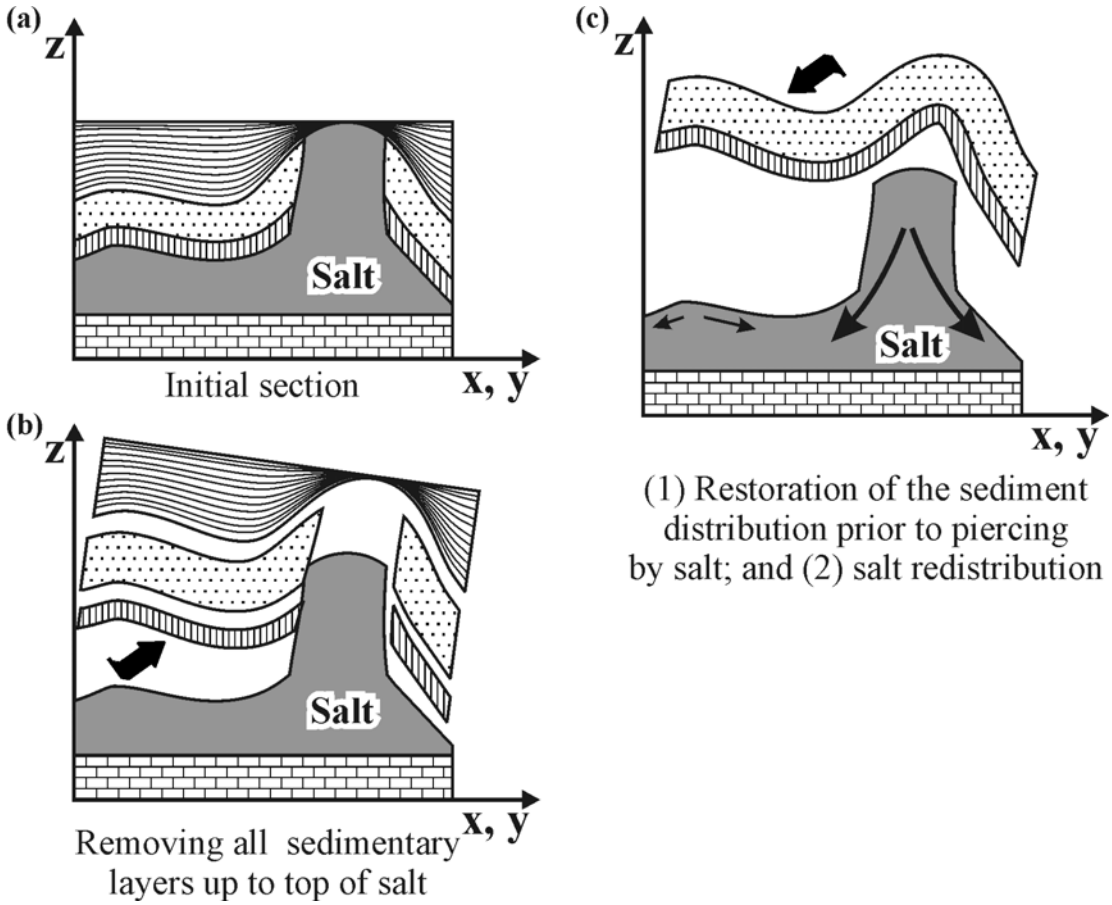

Figure 5.4. The schematic diagram shows a reconstruction of the sediment thickness prior to postdepositional erosion, allowing salt redistribution from the salt structure at the selected stratigraphic level (modified after Scheck et al., 2003).

Local postdepositional erosion of the sediments in the GG occurred during the main phases of salt tectonics which took place in the Triassic, Jurassic and during Tertiary. In addition, the area under consideration was affected by regional Late Jurassic-Early

Cretaceous erosion. Therefore, part of sediments is missing due to erosion and has to be re-established prior to salt redistribution for selected time steps. In order to solve this problem, the reconstructed sediment distributions were introduced as additional input data in terms of thickness maps. The reconstruction of the primary isochore maps was mainly based on the interpretation of seismic lines and published structural data from the GG (Baldschuhn et al., 1996; Baldschuhn et al., 2001; Kockel, 2003). The primary sediment distributions have been re-established for selected intervals, such as Triassic, Jurassic, Lower Cretaceous, Upper Cretaceous and Paleogene.

5.3.2.1. Triassic

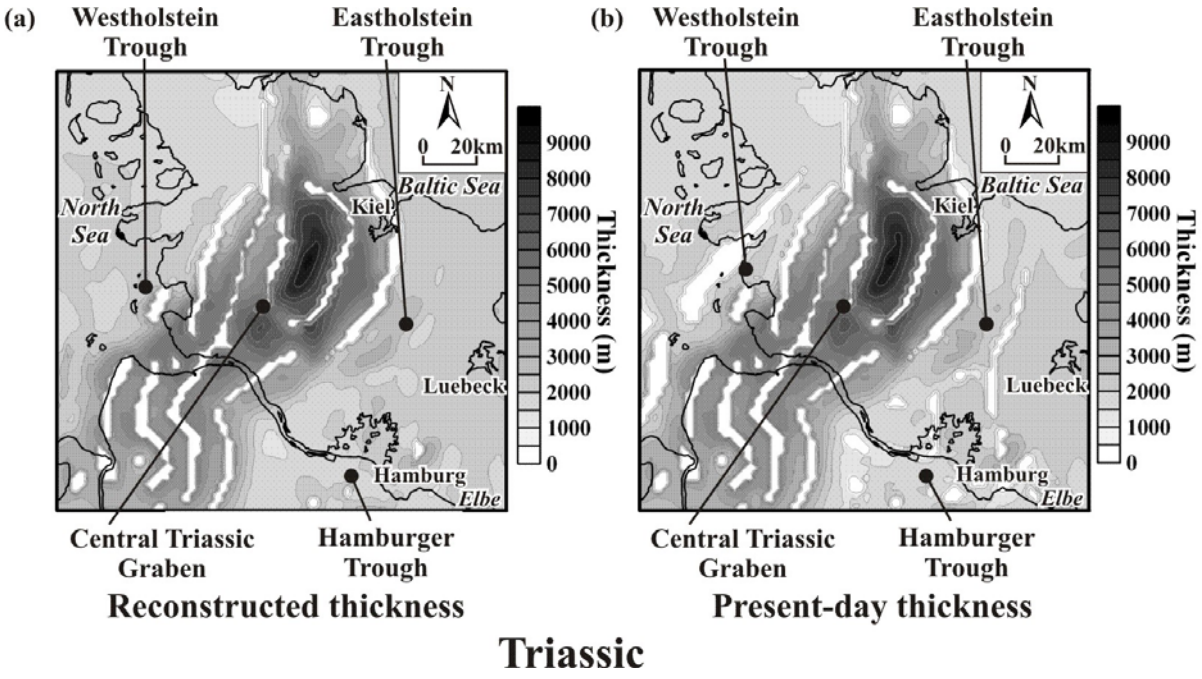

Figure 5.5. Thickness maps of the Triassic: (a) reconstructed to the end of the Triassic; and (b) present-day.

The reconstructed and present-day thickness maps of the Triassic are shown in Fig. 5.5. It is inferred from wells and seismic data that Triassic sediments were affected by Late Jurassic-Early Cretaceous regional erosion (e.g. Fig. 3.13b). The effect of the Late Jurassic-Early Cretaceous erosion was not strong because Triassic sediments were covered by

Jurassic prior to truncation. During this erosion, Triassic deposits were mainly eroded in the crests of salt structures where sediments were elevated higher than elsewhere by salt flow (e.g. Figs. 3.3a, 3.13b). In addition, post Triassic salt movements pierced Triassic sediments within the West-, Eastholstein and Hamburger Troughs. The effects of the postdepositional piercing and the Late Jurassic-Early Cretaceous erosion were taken into account for the reconstruction of the initial distribution of the Triassic sediments. In order to produce a reconstructed thickness map (5.5a), the present-day thickness map of the Triassic (Fig. 5.5b) has been corrected by re-interpolation of the areas where Triassic deposits are pierced and/or eroded. The greatest difference between the present-day and the reconstructed maps is visible within the marginal troughs. On the reconstructed map, the distribution of the Triassic sediments within the West-, Eastholstein and Hamburger Troughs has been re-established at the pre Jurassic state. Therefore, the position of the post Triassic salt structures is not shown as it is seen in Fig. 5.5b. On the other hand, salt walls and diapirs are still recognizable within the central part of the basin because their development occurred simultaneously with Triassic sedimentation. This is supported by seismic and borehole data which indicate that the Permian salt was extruded and even redeposited during latest Middle-Late Triassic (Keuper) time (see Chapter III). It is important to note, that the effect of post Triassic movements of the Keuper salt was not taken into account during the reestablishment of the initial distribution of sediments. In other words, Keuper salt movements have not been considered for the reason that it is impossible to separate the Keuper salt from the Permian salt within the salt structures. Therefore, the restoration of the initial thickness distribution of the Keuper salt has been neglected in the modelling process.

5.3.2.2. Jurassic

The restoration of Jurassic sediments prior to Late Jurassic-Early Cretaceous erosion is a more problematic task than the reestablishment of the Triassic thickness map. Figure 5.6 demonstrates the reconstructed and present-day thickness maps of the Jurassic. In the some parts of the GG, the entire Jurassic and lowermost Cretaceous sequences are missing (Fig. 5.6b). From the seismice data, it is not possible to decide whether the unconformity is erosive or non-depositional within the areas where sediments are lacking. Furthermore, many questions remain unresolved concerning the origin of the marginal troughs (Hamburger, West- and Eastholstein) where up to 1900-2400 m of Jurassic sediments were

accumulated (Fig. 5.6). Sanemann (1968) postulated that the formation of the marginal Jurassic rim-synclines occurred as a consequence of the Keuper extension by subsequent wave-front-like growth of salt stocks in post-Triassic times. In other words, the salt-induced deformation persisted in the Jurassic when rapid subsidence continued mainly around the former Triassic salt structures by gravity driven flow. This concept is not strictly consistent with the onlap patterns of the Jurassic sediments at the top of the Keuper succession (see Figs. 3.5, 3.8 and 3.10) indicating essential changes of the sedimentation style during the Jurassic. Kockel (2002) has documented the Early Jurassic extension and related normal faulting affecting the entire sedimentary succession within the Lower Saxony Basin and the Pompeckj Block. Although, there is no direct evidence of normal faults in the Jurassic of the

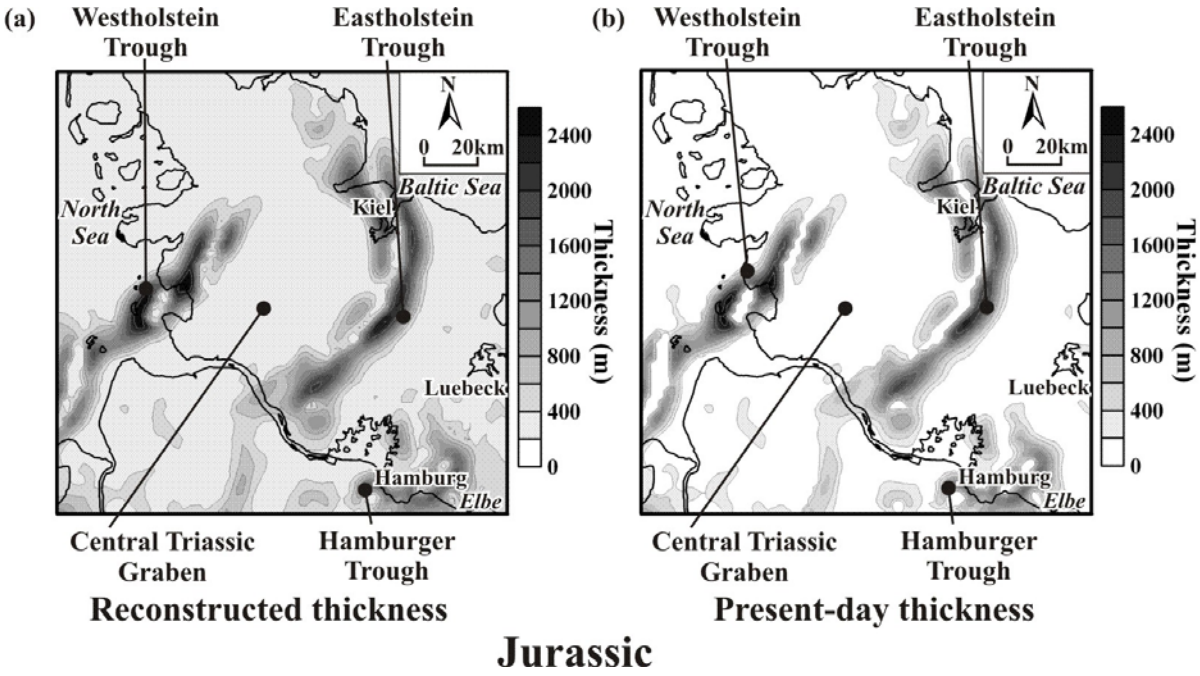

Figure 5.6. Thickness maps of the Jurassic: (a) reconstructed prior to the Late Jurassic-Early Cretaceous erosion; and (b) present-day.

GG, one of them can be inferred from structural features of the Jurassic strata in the Figure 3.8. Therefore, the Jurassic tectonic event documented in the Lower Saxony Basin and within the Pompeckj Block (Kockel, 2002) may have also affected the GG. However, post-Keuper salt tectonics occurred mainly along the north-western and the south-eastern margins of the GG (Figs. 1.4b and 3.2) where Permian salt was not depleted during the

Triassic. Thick Jurassic sediments are only observed around salt structures and are thinning away from salt walls or salt stocks (Figs. 3.2, 3.6, 3.9, 3.10, 3.13). Possibly, essential parts of the Jurassic might be missing due to erosional truncation in the Late Jurassic-Early Cretaceous. However, the Keuper strata were eroded mainly in the vicinity of salt structures (Figs. 3.3 and 3.9) or are transgressivlly covered by Lower Cretaceous sediments (for example see Fig. 3.3 and the NW part of the line 10 in the Fig. 3.10). The low degree of erosion of the Keuper (only up to the first hundred meters), the presence of truncated toplaps within the Jurassic strata (Figs. 3.5 and 3.9), and the absence of visible unconformities within the NW flank of the basin (Fig. 3.3), suggest a low degree of erosion rather than a strong uplift during Late Jurassic-Early Cretaceous times. In order to produce a reconstructed thickness map of the Jurassic (Fig. 5.6a), a constant value of 250 m was added to present-day thickness map. The constant value of 250 m was chosen in order to cover the entire region by sediments rather than to provide the true amount of the eroded sediments. This was done because the pattern of sediment distribution prior to erosion and postdepositional changes are unknown in detail. However, it is possible to suggest that the present-day thinning of the Jurassic sequence could reflect the proximal depositional limit with little Late Jurassic-Early Cretaceous erosion near rising salt structures. Thus, the erosional features did not extensively modify the ratio of thickness distribution of the depositional sequences in the Jurassic. Furthermore, the present-day remains of thick Jurassic still represents the areas of intensive subsidence, which was strongly controlled by withdrawal of the Permian salt from the source layer. Consequently, the reconstructed map in Fig. 5.6a can be taken as a qualitative approximation of the sediment distribution prior to erosion. On the other hand, it is obvious that the quantitative characteristic of the reconstructed thickness is poorly estimated due to an uncertainty of spatial and temporal changes in Late Jurassic-Early Cretaceous erosion rates and volumes.

5.3.2.3. Lower Cretaceous

The distribution of Lower Cretaceous deposits was only affected by post Cretaceous development of some salt structures, which pierced the sedimentary cover during the Tertiary. Therefore, the reestablishment of the Lower Cretaceous thickness map (Fig. 5.7a) was done by filling those areas, which have been pierced by post Cretaceous salt walls and diapirs (Fig. 5.7a). Consequently, the difference between reconstructed (Fig. 5.7a) and

present-day thickness maps (Fig. 5.7b) of the Lower Cretaceous is only the absence of pierced areas on the re-established sediments distribution.

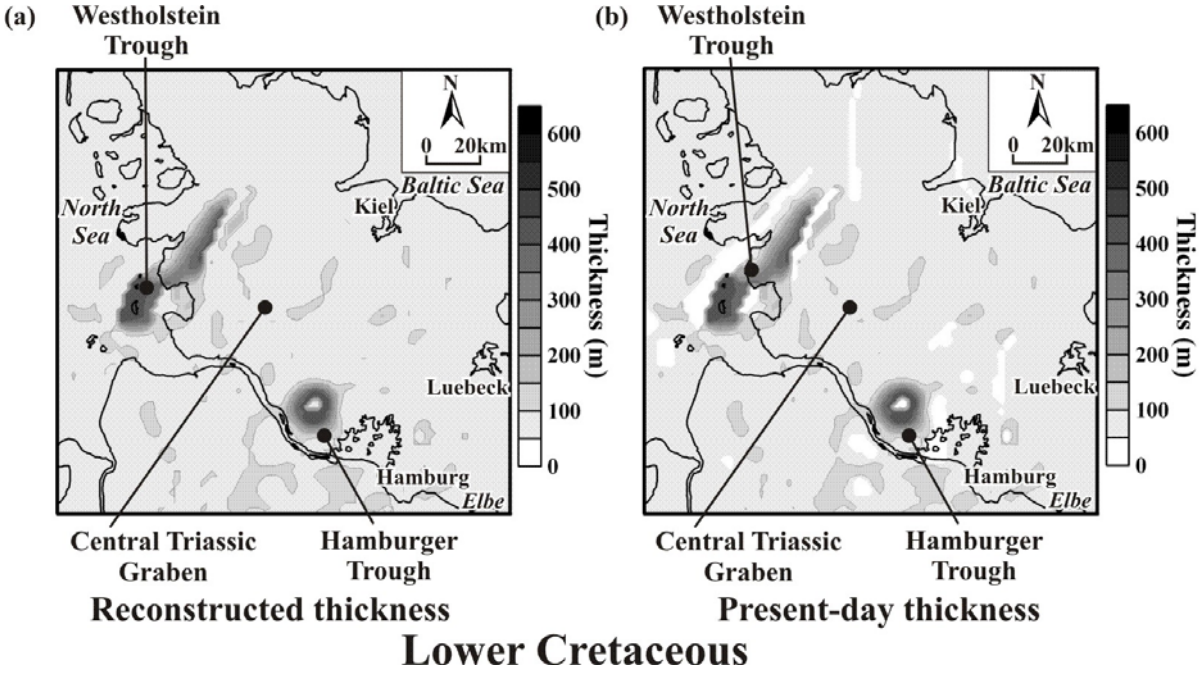

Figure 5.7. Thickness maps of the Lower Cretaceous: (a) reconstructed to the end of the Early Cretaceous; and (b) present-day.

5.3.2.4. Upper Cretaceous

The reconstructed and present-day thickness maps of the Upper Cretaceous are shown in Fig. 5.8. It was inferred from seismic data that the deposition of the Upper Cretaceous took place under tectonically quiescent conditions (see Chapter III). There are no indications of strong salt movements during the Late Cretaceous in the area under consideration. Therefore, the presence of holes due to piercing by salt walls and diapirs is a result of post Cretaceous salt movements. Like for the Lower Cretaceous, pierced regions were removed from the present-day thickness map (Fig. 5.8b) by reinterpolation of those areas which correspond to the present-day position of post Cretaceous salt walls and diapirs. In addition, Upper Cretaceous sediments were deformed, uplifted and partially eroded within the crest of some salt structures during postdepositional times (e.g. Figs. 3.2, 3.7-3.10). These features are easily seen on the present-day thickness map (Fig. 5.8b) due to the

presence of locally decreased thickness of the Upper Cretaceous. These areas were

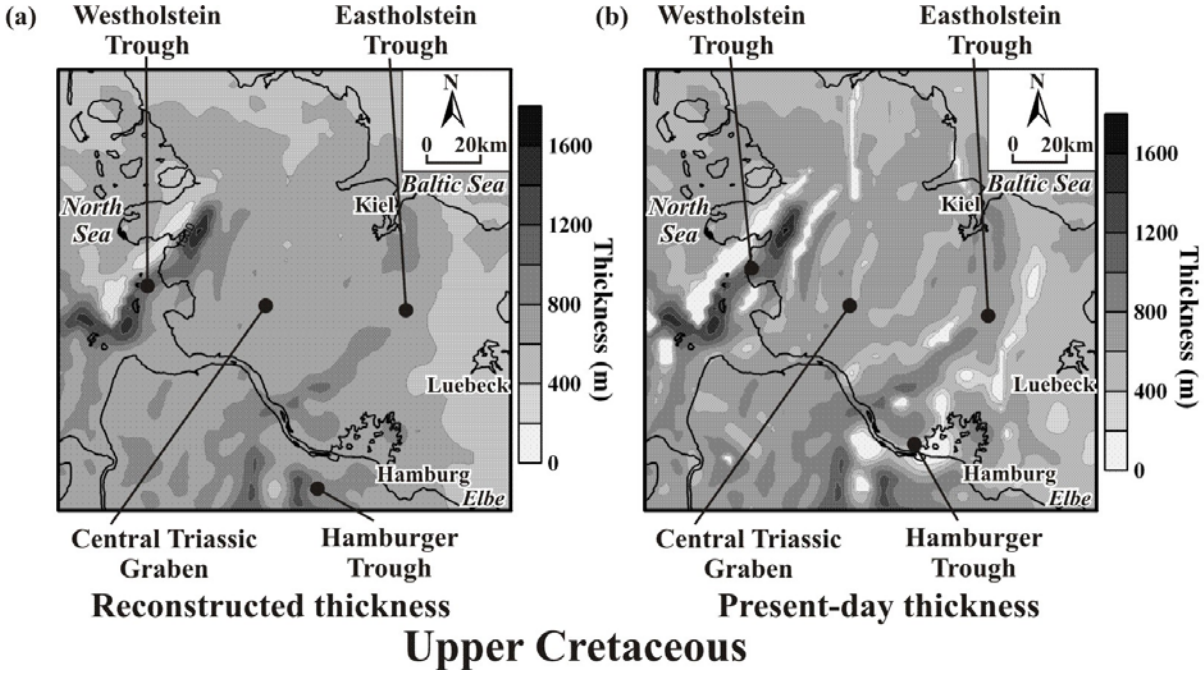

Figure 5.8. Thickness maps of the Upper Cretaceous: (a) reconstructed to the end of the Late Cretaceous; and (b) present-day.

reinterpolated in order to remove the effect of the salt induced postdepositional erosion above the salt structures. On the reconstructed map (Fig. 3.8a), the distribution pattern of the Upper Cretaceous is characterized by almost constant thickness with exception of two areas within the Westholstein and Hamburger Troughs (Fig. 5.8a). These two areas of the decreased thickness correspond to two salt structures, which were active during the Late Cretaceous. There, the structural features indicate that the deposition of the thick Upper Cretaceous took place simultaneously with salt movements within relatively shallow rim synclines (see Chapter IV for details). Therefore, the formation of the Upper Cretaceous rim synclines requires partly decreased thicknesses in the limit of the simultaneously growing salt structures.

5.3.2.5. Paleogene

It is inferred from seismic data (Chapter III) and published structural data (Baldschuhn et al., 1996; Baldschuhn et al., 2001; Kockel, 2003) that the deposition of the Paleogene was accompanied by simultaneous development of salt structures. Some salt structures pierced the sedimentary cover at that time within the West-, Eastholsein and Hamburger Troughs. The effect of syndepositional growth of salt structures is visible by the presence of locally increased thickness around salt structures (Fig. 5.9b). In addition, Neogene growth of salt structures caused partial erosion of the Paleogene sediments within the crest of the salt anticlines and walls. During the reconstruction of the Paleogene thickness, the main attempt focussed at the reestablishment the Paleogene thickness within the crest of salt structures prior to Neogene. The result of the reconstruction of the Paleogene sediment distribution is shown in Fig. 5.9a. The thinning of the Paleogene in the crests of salt structures is smoothed on the reconstructed thickness map (Fig. 5.9a) in comparison to the present-day thickness map (Fig. 5.9b).

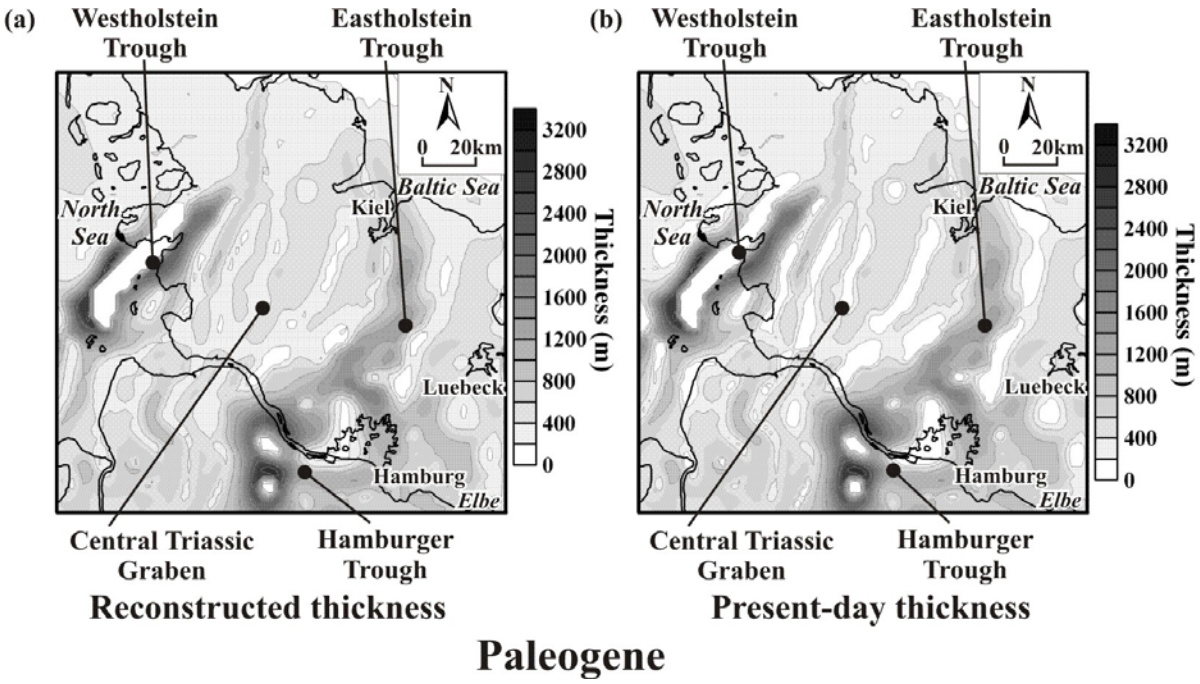

Figure 5.9. Thickness maps of the Paleogene: (a) reconstructed to the end of the Paleogene; and (b) present-day.

5.3.3. Results of the modelling

The results of reverse modeling are shown in Figs. 5.10 and 5.11 (see enlardged versions in Appendix B). 3D views of the top of the Permian salt at the different stratigraphic levels are plotted in Fig. 5.10, in order to allow easier visual perception of changes in geometry of salt structures through time. The obtained results show substantial change of the salt structure distribution from the end of theTriassic (Fig. 5.10f) to present-day (Fig. 5.10a). The results support the conclusion that initial salt movements took place during Middle-Late Triassic within the central part of the GG (Fig. 5.10f). Fig. 5.10f also indicates the development of mainly shallow salt anticlines within the marginal troughs in the Triassic. Following its initiation, strong salt tectonics occurred at the margins of the former Triassic Graben in the Jurassic (Fig. 5.10e). During the Cretaceous-Tertiary, the salt structures were affected by additional growth mainly within the marginal troughs (Figs. 5.10a-d). The evolution of salt structures can be explained in more details by changes of salt thickness, as derived during the reverse modelling. Fig. 5.11 illustrates the modelled thickness of Permian salt for the present-day state and for different stages of backstripping. One of the most remarkable results of the 3D structural model is related to the expansion of the depletion zone or reduced thickness of the Permian salt, which is shown by white colour in Fig. 5.11. It is clearly seen that the Permian salt layer was almost depleted within the central part of the basin in the Triassic (Fig. 5.11f). A small area of the reduced thickness of the salt is also seen west of Hamburg (Fig. 5.11f), indicating Triassic salt movements within the Hamburger Trough. The marginal troughs (West-, Eastholstein and Hamburger) are characterized by locally increased salt thickness, which can be related to salt anticlines. During the Jurassic, the reduction of the salt layer extended onto the SW and NE margins of the Central Triassic Graben (Fig. 5.11e). The zone of reduced thickness within the Hamburger Trough became wider in comparison to Triassic times (cf. Figs. 5.11f and 5.11e). The difference between the salt distribution in the Jurassic (Fig. 5.11e) and in the Cretaceous (Figs. 5.11c, d) is smoothed or even not visible in most parts of the basin, proving low salt activity in the Cretaceous, which was already inferred from the interpretation of seismic lines in Chapter III. Only some inessential reductions of the salt thickness are recognizable within the Westholstein and Hamburger Troughs in addition to those, which are observed in the Jurassic. The next stage of the strong broadening of the area of highly reduced salt thickness

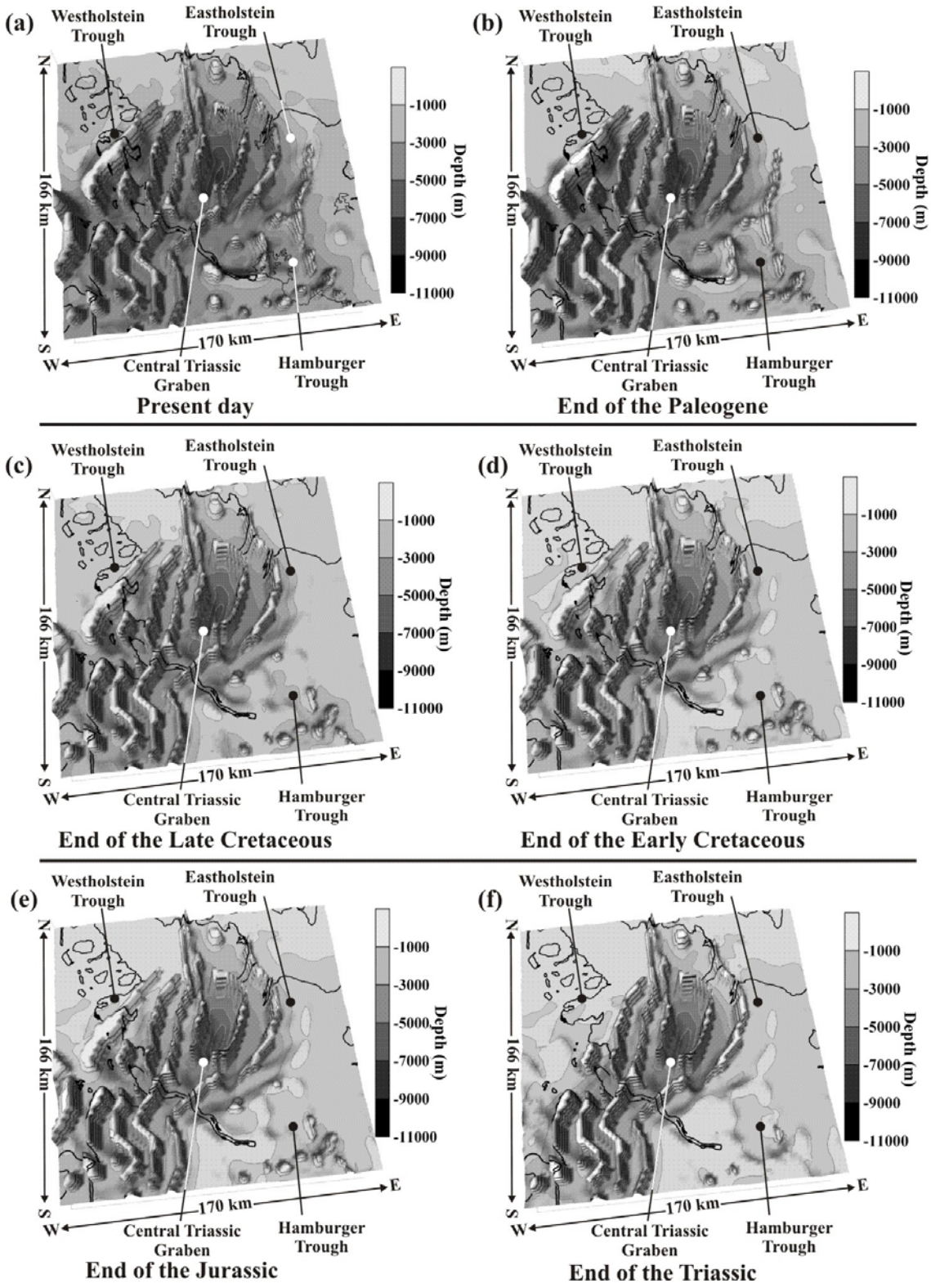

Figure 5.10. 3D views on the top of the Permian salt at the different stratigraphic levels as result of reverse modelling. Evolution of salt structures is shown from the end of the Triassic (f) to present-day (a).

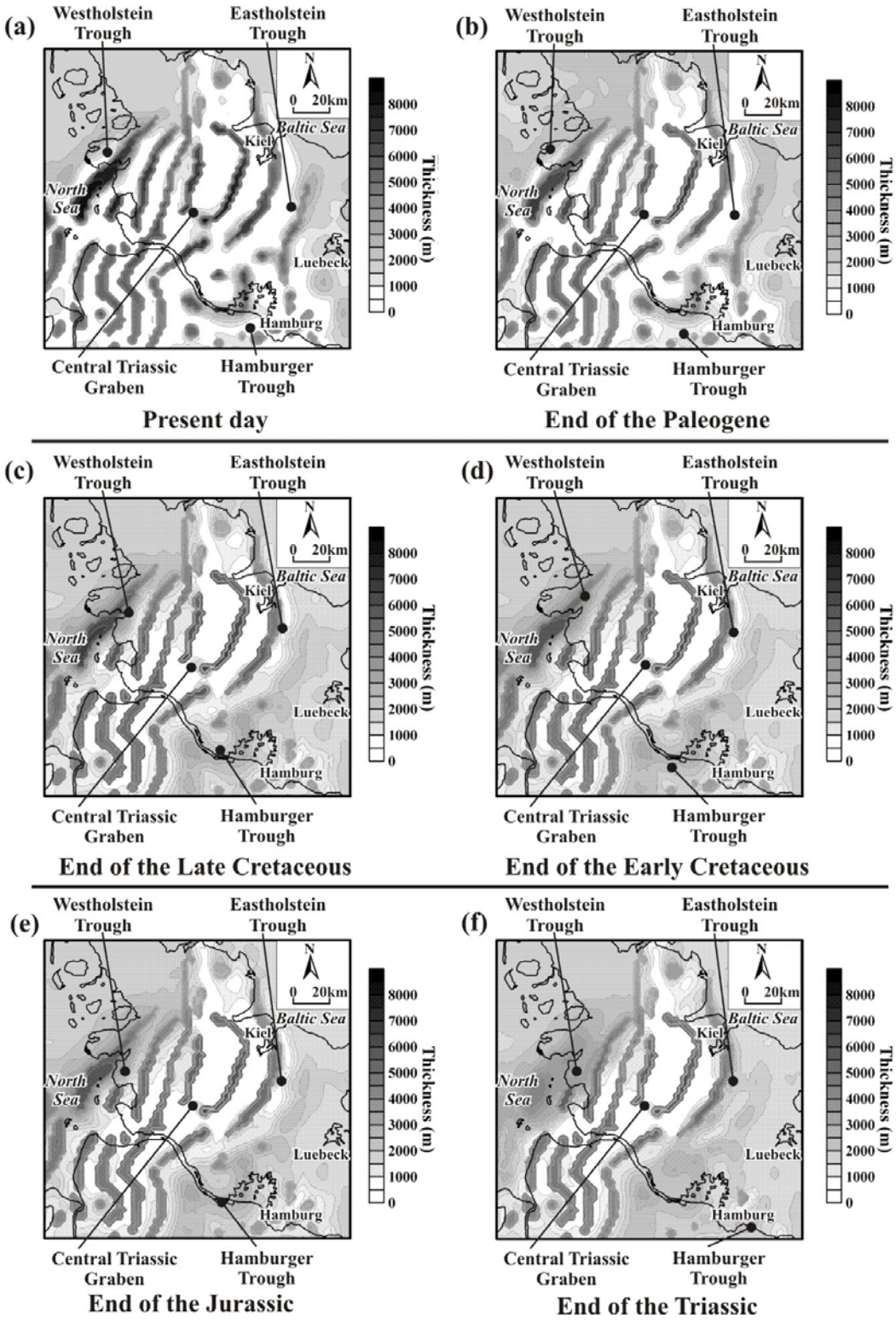

Figure 5.11. Isochore maps of the Permian salt representing thickness distribution of the salt from the end of the Triassic (f) to present-day (a) based on reverse modelling. Gradual movements of the depletion zone of Permian salt from the central part of the original Central Triassic Graben (f) towards its margins (a) is shown by white colour.

is shown in Fig. 5.11b. The map of salt thickness at the end of the Paleogene demonstrates that the depletion of the Permian salt layer occurred mainly within the marginal troughs. During the Paleogene, the thickness of the salt was strongly reduced within the West- and Eastholstein Troughs. On the other hand, depletion of the salt layer within the Hamburger Trough was stronger on the western and eastern parts of this trough than in the central part (Fig. 5.11b). Fig. 5.11a demonstrates further expansion of the salt depletion zone towards the basin flanks during the Quaternary-Neogene.

The 3D geometries of the reconstructed salt structures in Fig. 5.10 are reflected in the reduction of the salt thickness (Fig. 5.11) from the end of the Triassic to the present-day. In other words, the 3D reverse modelling provides evidence for depletion of the Permian salt layer from the central part of the basin towards the basin flanks. Reverse modelling is in agreement with the predicted development of salt structures, which was inferred from seismic lines and present-day sediments distribution in the GG (see Chapters III and IV).

According to the results of the 3D reverse structural modelling, the formation of the deep Central Triassic Graben and the subsequent Jurassic-Cenozoic marginal troughs was partially controlled by gradual depletion of the Permian salt layer through time.

5.4. Results of 3D forward modelling

The modelling approach aims to reconstruct the original Permian salt distribution immediately after deposition. The concept of the 3D forward modelling is illustrated by a 2D schematic diagram in Fig. 5.12. Fig. 5.12a represent the present state of the model. The reconstruction of the initial thickness of salt was carried out in the following sequence. The first step is backstripping of the Meso-Cenozoic sediments and the Permian salt (Fig. 5.12b). After that, the isostatic response of the salt base without sediment infill was calculated (Fig. 5.12c). The restoration of the Permian salt layer above the backstripped and isostatically balanced base of salt is the third step of modelling (Fig. 5.12d). The reconstruction of the initial salt thickness takes into account that the Permian salt partially extruded during the Keuper and was redeposited due to superficial dissolution. The quantity of Permian salt redeposited during the Keuper can be approximately derived from lithostratigraphic and

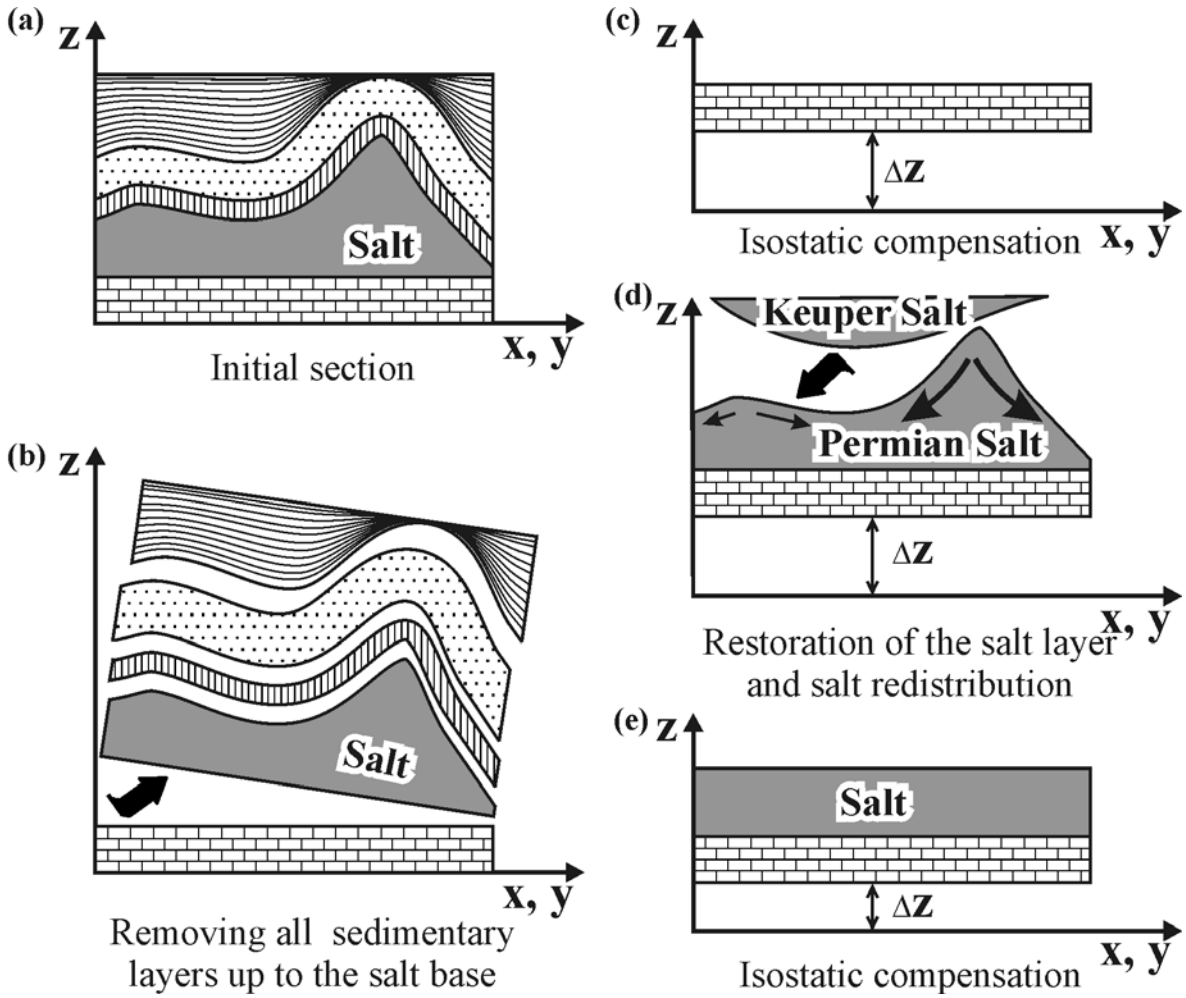

Figure 5.12. Schematic diagram showing different steps of the forward modelling.

structural features of the Keuper succession, which are described in details in Chapters II and III. The amount of salt in the Keuper has been estimated as twenty percentages of the thickest part of the section which occupies the central part of the GG (Fig. 5.13b). Subsequently, the redeposited Permian salt (20% of thickest Keuper) was added to the Permian salt (Fig. 5.12d). The next step is the redistribution of the total Permian salt onto the restored base like a viscous fluid until the salt layer was in hydrostatic equilibrium (Fig. 5.12d) and, finally, the calculation of an isostatic response due to the new load conditions which caused by renewed distribution of salt (Fig. 5.12e).

The obtained initial thickness is displayed in Fig. 5.13c. It shows a spatial correlation between two modelled maxima of the initial salt thickness distribution (Fig. 5.13c)

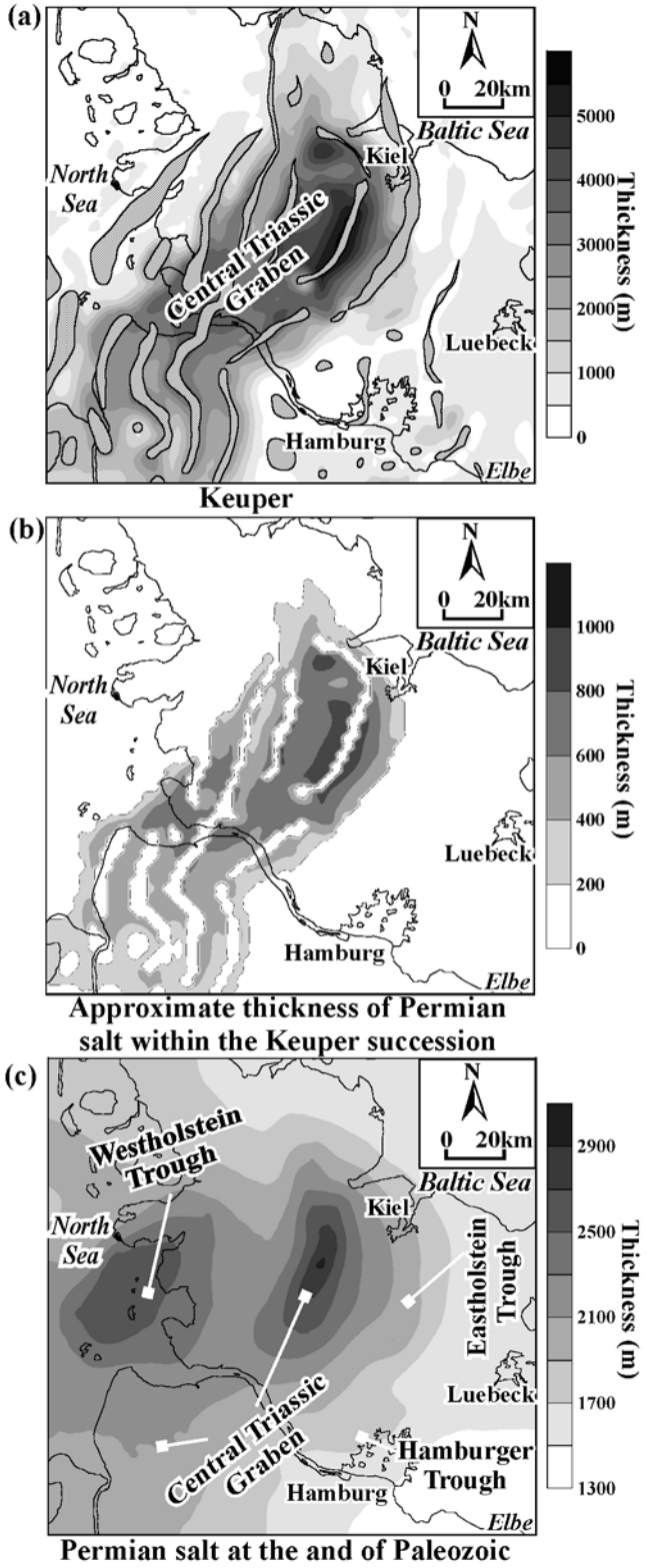

Figure 5.13. (a) Thickness map of the uppermost Middle Triassic and Upper Triassic (Keuper); (b) suggested thickness of the Permian salt within the Keuper strata; (d) reconstructed map of initial salt thickness obtained from 3D salt redistribution within the studied area.

and present-day depth minima within the Westholstein trough and the central part of the GG (Fig. 4.2c). The modelled two maxima of initial salt thickness are correlated with the present-day salt distribution, which is characterized by the largest salt walls within the Westholstein Trough and in the Central Triassic Graben (Figs. 5.10a and 5.11a). The initial salt thickness varies from 1300 m at the flanks of the basin up to 3000 m within the central part. On the basin scale, a clear NNE-SSW trend of the GG is recognizable due to the presence of two NNE-SSW extended maxima of Permian salt thickness. The regional trend of the restored salt distribution points to a westward continuation of the Permian salt basin (Fig. 5.13c). The initial salt thickness varies from 1300 m at the flanks of the basin up to 3000 m within the central part. On the basin scale, a clear NNE-SSW trend of the GG is recognizable due to the presence of two NNE-SSW extended maxima of the Permian salt thickness. The regional trend of the restored salt distribution points to a westward continuation of the Permian salt basin (Fig. 5.13c). In addition, the map displayed in Fig. 5.13c shows that the relative low degree of salt-tectonic activity within the flanks of the basin may have been predetermined by relatively thin initial salt thickness. Thus, the initial thickness of the Permian salt may have controlled the structural style of the basin. Where salt was thick, salt diapirs were formed and the overburden was subjected to high-amplitude folding. Where salt was relatively thin, simple salt pillows and shallow anticlines developed.

Because the modelling approach assumes the volume of salt to be constant through time, the initial thickness of the Permian salt bears an error in the sense that a possible salt loss due to underground dissolution is not considered. The significance of this process is highlighted by Clark et al. (1999) and Cartwright et al. (2001) in the North Sea basin. Most probably, considerable superficial dissolution did occur not only in the Keuper but also in later times. On the other hand, some of the dissolved salt re-entered the system via redeposition during the Keuper – a process considered in the modelled salt volume. However, these aspects of the salt dissolution are too complex, preventing a reliable estimate of the dissolved Permian salt and therefore, have been postponed to future studies.

5.5. Summary

The results of the modelling reveal the thickness distribution of the Permian salt within the GG from the end of the Permian (Fig. 5.13c) to present-day (Fig. 5.11). Three phases of strong growth of the salt structures have been identified by 3D reverse modelling.

A major phase of growth occurred during the Triassic within the central part of the basin (Figs. 5.10f and 5.11f), which can be related to almost W-E extension in the Keuper. This activation of salt tectonics was followed by a Jurassic pulse of salt movements (Figs. 5.10e and 5.11e) which temporally correlates with an extensional event in the Pompeckj Block and the Lower Saxony Basin. The third, Paleogene-Neogene tectonic event caused significant growth and amplification of the salt structures mainly at the margins of the basin (Figs. 5.10 a, b and 5.11 a, b). This event is extensional with a possible horizontal component of tectonic movements. These three phases of salt tectonics were separated by intervals associated with very low degree of salt mobility in the Early and Late Cretaceous (Figs. 5.10 c, d and 5.11 c, d). Therefore, the results of the modelling indicate a good correlation between the main phases of salt movements and tectonic events in the area under consideration.

It is important to note that the restoration method has several sources of errors. The results of the salt redistribution depend strongly on the input data set, such as reconstructed thickness maps for reverse modelling and the shape of the base of the Permian salt for forward modelling. The method also depends how correctly the amount of Permian salt is determined. In order to avoid possible mistakes, the reconstructed thickness maps were established by using all available data, the shape of the salt base was predefined with some approximation beneath the salt structures and strong extrusion and dissolution of the Permian salt during Keuper was taken into account. Some errors of the modelling can occur as a result from an imprecisely constructed salt base beneath the salt structures and possible additional salt dissolution during the Mesozoic and Tertiary. Additionally, the re-established distribution of the Keuper sediments has to be corrected for postdepositional Keuper salt movements at the post Triassic evolution stage of the GG. All these uncertainties require individual investigations by use of additional data (seismic lines and deep wells), and therefore a unique solution of these uncertainties cannot be achieved in the present study. For instance, the prestack migration has to be applied to all seismic lines crossing salt walls in order to resolve a seismic image beneath salt structures; additional borehole data and seismic lines are needed for accurate correlation of reflections within the areas which are strongly affected by salt tectonics and so on. For that reason, some simplifications were used in the modelling process. In any case, the results of the modelling will not avoid all quantitative errors, and have to be considered as a first approximation. Therefore, 3D

structural modelling provides quantitative results in spite of some simplification due to a deficit of the existent and/or available geological and geophysical data.

In summary, it can be stated that the development of the depletion zone of the Permian salt through time (Fig. 5.11) is in agreement with the observed distribution of the maximum subsidence centres of the different stratigraphic units (Fig. 4.13). In the central part of the GG, the depletion occurred already in the Triassic and it is perfectly correlated with the thickest Triassic (cf. Figs. 5.11f and 4.13). During the Jurassic, Cretaceous and Tertiary, the areas of depleted Permian salt shifted towards the basin flanks and the same occurred with the centres of maximum subsidence. Only minor isolated salt pillows remained within the central part of the basin and have locally fed salt walls and diapirs during post Triassic time. The sedimentation centres for each time stage are always located above the zone of the reduced or depleted Permian salt. Thus, the results of the modelling show that salt withdrawal may have played an important role during the Meso-Cenozoic evolution and that the effects of the salt-driven subsidence during the Meso-Cenozoic may be considered a main reason for the formation of the deep Central Triassic Graben and the subsequent Jurassic-Cenozoic marginal troughs.